Chinese Chemical Letters 34 (2023) 107203

Contents lists available at ScienceDirect

Chinese Chemical Letters

journal homepage: www.elsevier.com/locate/cclet

Tb^{3+}-xylenol orange complex-based colorimetric and luminometric dual-readout sensing platform for dipicolinic acid and metal ions

Lixia Lu[a,*], Xinyu Shao[a], Xiaoxiao Lin[a], Linhe Ding[a], Bingchan Song[a], Jian Sun[b,*]

[a] Shandong Provincial Key Laboratory of Animal Resistance Biology, Institute of Biomedical Sciences, Key Laboratory of Food Nutrition and Safety of Shandong Normal University, College of Life Science, Shandong Normal University, Ji'nan 250014, China
[b] State Key Laboratory of Electroanalytical Chemistry, Changchun Institute of Applied Chemistry, Chinese Academy of Sciences, Changchun 130022, China

ARTICLE INFO

Article history:
Received 6 December 2021
Revised 9 January 2022
Accepted 7 February 2022
Available online 9 February 2022

Keywords:
Lanthanide complex
Xylenol orange
Bacillus anthracis
Multiple detection
Linear discriminant analysis

ABSTRACT

A dual-readout sensing platform based on two signal transduction channels can integrate the unique advantages of each sensing pattern, compensate for the deficiency in the adaptive capacity, and enable a more convincing performance in analytical applications. Here, we introduce a responsive molecule dye, xylenol orange (XO), to combine with lanthanide terbium ions (Tb^{3+}). The resultant Tb^{3+}-XO complex exhibited tunable optical properties and was used as a novel colorimetric and luminometric dual-readout sensing platform for assaying the anthrax biomarker, dipicolinic acid (DPA). In the presence of Tb^{3+}, the XO solution underwent a color change from yellow to magenta; however, upon adding DPA, the color changed back to yellow immediately, accompanied by the characteristic luminescence emission of Tb^{3+}. Considering the strong affinity between DPA/XO and metal ions, the proposed sensing platform was further employed for the determination and differentiation of certain metal ions using linear discriminant analysis. This convenient dual-readout sensing platform offers several notable features and significantly promotes the application and development of lanthanide-based materials.

The unique electronic structure and physicochemical properties of lanthanide elements provide a strong foundation for their wide application. Because of the long luminescence lifetime, large Stokes shift, and sharp linear emission caused by the f-f forbidden transition [1], lanthanide-based materials find application not only in lighting, displays, and optical communication signal amplification, but also in luminescence immunoassays, cell imaging, and magnetic resonance imaging tracing [2–4]. The past decades have also witnessed the rapid development of lanthanide complex-based luminescent probes, especially terbium ions (Tb^{3+}) and europium ion (Eu^{3+}) complexes [5–10]. The rich ligand designability of lanthanide complexes allows for tunability according to the required functions. Coupled with the characteristics of lanthanide luminescence, lanthanide complexes offer unique advantages in the design of molecular probes or sensing platforms.

Dipicolinic acid (DPA, also known as pyridinedicarboxylic acid), which is widely prevalent in bacterial spores and accounts for 5%–15% of the total dry mass of bacterial spores, has been used as a biomarker for detecting *Bacillus* and *Clostridiu* [11,12]. These spores can survive in extreme environmental conditions such as those with high temperatures, chemical disinfectants, and radiation. *B. anthracis* in *Bacillus* is extremely toxic; it has been reported that the inhalation of over 10^4 *B. anthracis* spores can be fatal if timely and effective treatment is not provided [13–19]. Therefore, the sensitive, rapid, and accurate detection of DPA are crucial to avoid food poisoning and potential bioterrorism.

Among the series of current analytical detection means, colorimetric and luminescent methods are most sought after because the results are visible to the naked eye and the analyses do not require complex instrumentation [12,20]. In this regard, lanthanide-based luminescent sensors such as lanthanide-doped metal organic frameworks (MOFs) and coordination polymer nanoparticles for DPA detection have been reported [11,21–23]. However, most sensors are based on the absolute change in the luminescence intensity of lanthanide ions; further, such single-modal readout signals are susceptible to environmental or instrumental fluctuations. In contrast, an integrated dual-readout platform would overcome these limitations [24], and combine the simplicity of colorimetric methods with the higher sensitivity of luminescent methods [1,25]. In fact, multifarious designable ligands and ligand displacement methods based on lanthanide complexes could be promising to develop a dual-readout strategy with higher accuracy, making them an alternative and better choice for DPA detection [19,26,27]. Moreover, owing to the strong affinity between DPA and metal ions, it is

* Corresponding authors.
E-mail addresses: lulixia@sdnu.edu.cn (L. Lu), jiansun@ciac.ac.cn (J. Sun).

https://doi.org/10.1016/j.cclet.2022.02.009
1001-8417/

worth exploring the potential for the recognition of metal ions. It is well known that metal ions play vital roles in biological processes, and a deviation from normal levels usually leads to the occurrence and progression of diseases such as neural malfunction or cancers [28,29]. Consequently, the detection of metal ions, particularly the rapid discrimination and determination of multiple metal ions, has attracted significant research focus.

The organic dye xylenol orange (XO) is a well-known metal chelating agent that has previously been used as an antenna to form stable luminescent coordination complexes with Yb^{3+} and provide near-infrared luminescence [30]. It possesses strong absorption in the visible range, and is yellow in an acidic solution and magenta in an alkaline solution, thus it can also serve as a responsive molecule. Despite these properties, XO has rarely been combined with lanthanide-based materials. Inspired by these facts, we introduced XO to successfully construct a Tb^{3+}-XO complex and elucidated its formation process, binding mode, and optical properties for the first time. The XO-Tb^{3+} binary complex was further employed as a novel colorimetric and luminescent dual-signal sensing platform for assaying DPA. In a weak acidic medium, DPA displaced XO in the XO-Tb^{3+} complex and combined with Tb^{3+} to sensitize the green luminescence of Tb^{3+}, accompanied by a color change of the solution from magenta to yellow. Thus, the dual-signal quantitative detection of DPA with high sensitivity and selectivity can be realized. Moreover, the above system was further used to detect diverse metal ions and investigate outcomes considering the strong affinity between DPA/XO and metal ions [31,32]. Interestingly, different metal ions caused varying degrees of luminescence and color change, allowing the identification and detection of these metal ions using linear discriminant analysis (LDA).

The dual colorimetric and luminometric assays for DPA and metal ions are outlined in Scheme 1. Tb^{3+} was selected because it exhibits a greater binding affinity to dipicolinate among common luminescent lanthanides [11]. The UV–vis spectrum in Fig. S1A (Supporting information) shows that XO has maximum absorbance at 430 nm and the color is yellow. With the consecutive addition of Tb^{3+} ions from 0 μmol/L to 15 μmol/L, the absorbance at 570 nm increased gradually and decreased at 430 nm, and the color of the solution changed from yellow to magenta, indicating the formation of the Tb^{3+}-XO complex. Multiple atoms in the XO molecule can participate in coordination; however, only when the phenolic oxygen atom coordinates with metal ions is an appreciable color change possible [33]. Therefore, we speculate that coordination occurs between Tb^{3+} and XO as depicted in Scheme 1, to form a 1:1 complex. The association constant using a 1:1 binding model for the Tb^{3+}-XO complex (Fig. S1B in Supporting information) was calculated to be $10^{5.35}$ (Fig. S2 in Supporting information), which is 100 times lower than that of the DPA-Tb^{3+} complex [11], ensuring the success of the ligand displacement strategy. Job's plot was obtained to characterize the binding stoichiometry, and further confirmed the 1:1 binding mode for the Tb^{3+}-XO complex, as shown in Fig. S1C (Supporting information).

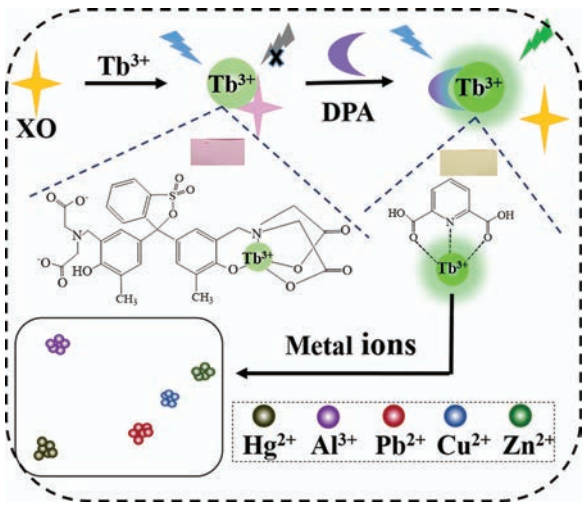

Scheme 1. Schematic of the colorimetric and luminescent assay for DPA and metal ions.

The absorption spectra of the Tb^{3+}-XO complex with the consecutive addition of DPA were recorded and are displayed in Fig. 1A. As the concentration of DPA continued to increase, the absorbance increased at 430 nm and decreased at 570 nm; simultaneously, the color of the solution returned from magenta to yellow, demonstrating the displacement of XO by DPA from the Tb^{3+}-XO complex. A drastic color change occurred instantaneously, which was easily visible to the naked eye.

Fig. 1B shows the absorbance ratio (A_{430}/A_{570}) against the concentration of the added DPA. The ratio continued to increase with the increase in DPA concentration, and was linearly correlated with the DPA concentration in the range of 0–8 μmol/L. The lowest detection concentration was 1 μmol/L, which is much lower than the infectious dose of bacterial spores (60 μmol/L).

Next, we investigated the luminescence response of the Tb^{3+}-XO complex to DPA. For greater sensitivity, the excitation wavelength was optimized to be 225 nm, as shown in Fig. S3 (Supporting information). The emission peaks at 490, 545, 585 and 621 nm are typically the characteristic peaks of Tb^{3+}, and the luminescence intensity is highest at 545 nm, corresponding to the $^7F_5 \rightarrow {}^5D_4$ transition. DPA undergoes intersystem crossing to a triplet state under 225 nm excitation, and selectively transfers the energy to Tb^{3+}. As shown in Fig. 1C, with an increase in the DPA concentration, the intensity of the emission peak at 545 nm showed an increasing trend, and the green luminescence color became increasingly pronounced. We also explored the effect of XO on the luminescence of Tb^{3+}, as shown in Fig. S4 (Supporting information). The introduction of XO failed to change the luminescence spectrum; however, once DPA was added, a significant enhancement in the luminescence intensity could be observed. This phenomenon indicated that XO was incapable of sensitizing Tb^{3+} to luminescence, which may be because XO could not absorb energy and transfer it to Tb^{3+} effectively under 225 nm excitation. Moreover, the luminescence response to DPA was completed instantaneously. Once the solution is mixed thoroughly, the luminescence spectra can be measured without a longer reaction time (Fig. S5 in Supporting information). Fig. 1D shows an S-shaped curve of the relationship between the DPA concentration and luminescence intensity at 545 nm. There is a linear relationship in the concentration range of 0–8 μmol/L and the limit of detection (LOD) was calculated to be 34 nmol/L ($3\,\sigma/S$). Table S1 (Supporting information) lists the comparison between this method and others for DPA detection, indicating that this method presents clear advantage on the whole.

To further explore the practicality of this method, we conducted experiments using the same procedures on several organic compounds with structures similar to that of DPA. The concentration of DPA shown in Fig. 1E was one-tenth that of the remaining organics. All the measured organic compounds had little effect on the luminescence intensity and UV–vis signal of the Tb^{3+}-XO complexes, while the system could selectively respond to DPA among the mixture of DPA and all other compounds. These results indicate that the displacement method is highly specific for the quantitative detection of DPA.

Soil was used as the experimental sample to further explore the reliability of this assay. The additive recovery method was employed to detect DPA in the soil samples, and the results are shown in Table S2 (Supporting information). The soil matrix had no significant effect on this detection system after appropriate

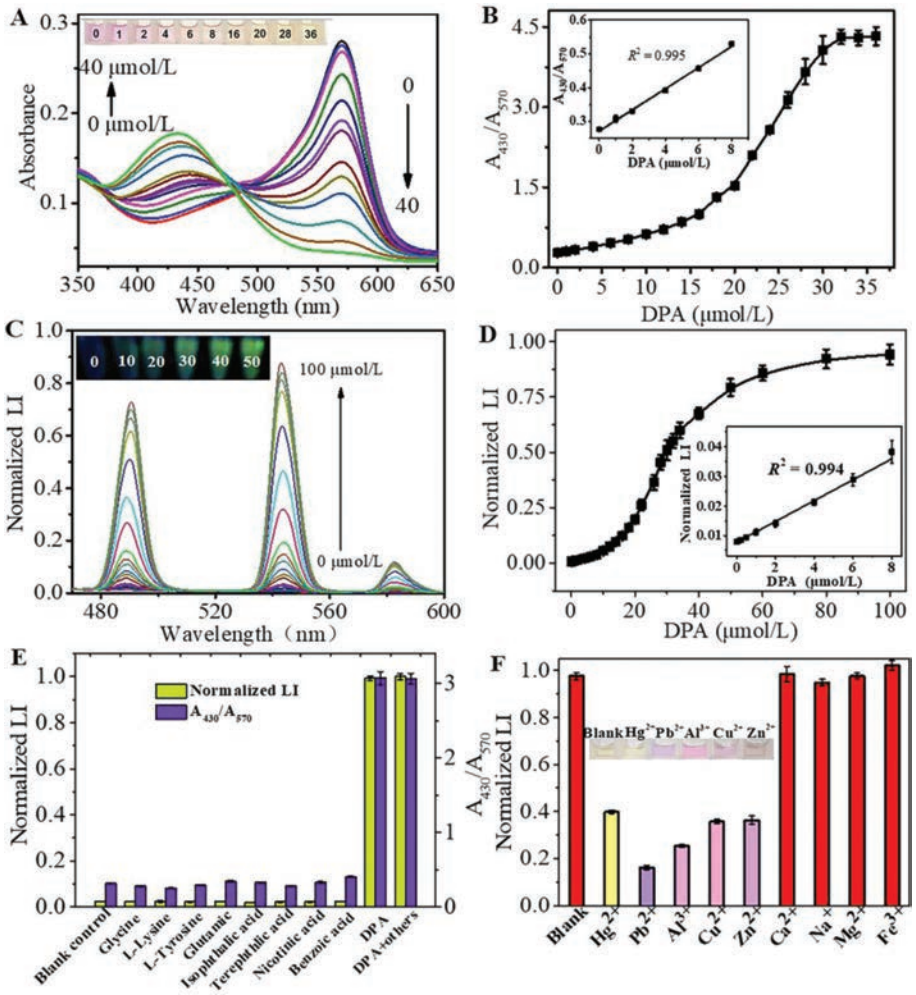

Fig. 1. (A) UV–vis spectra of XO-Tb^{3+} complex (15 μmol/L) with consecutive addition of DPA and a photograph (inset). (B) Change in the absorbance ratio (A_{430}/A_{570}) with the concentration of DPA and the linear relationship in lower concentration (inset). (C) Luminescence spectra of XO-Tb^{3+} complex (15 μmol/L) with consecutive addition of DPA and a photograph under 250 nm UV irradiation (inset). (D) Luminescence intensity at 545 nm against the concentration of DPA and the linear relationship in lower concentration (inset). (E) Effect of presence of competitive aromatic ligands (glycine, L-lysine, L-tyrosine, glutamic, isophthalic acid, terephthlic acid, nicotinic acid and benzoic acid) on the colorimetric and luminescent response of XO-Tb^{3+} complex. (F) Effect of common metal ions on the luminescence intensity of XO-Tb^{3+}-DPA system, and a visual photograph of the solution in the presence of Hg^{2+}, Pb^{2+}, Al^{3+}, Cu^{2+} and Zn^{2+}.

pretreatment. Subsequently, different amounts of standard solutions of DPA were added, and the recovery rates of DPA were measured as 93%, 103% and 91%, respectively. These satisfactory results confirm that the quantitative detection of DPA based on the Tb^{3+}-XO complex is reliable and has broad application prospects.

Considering the high affinity between DPA/XO and metal ions, we deduced that the further addition of specific metal ions to the Tb^{3+}-XO-DPA system may affect the luminescent or colorimetric signal, which could be used for the determination of the corresponding metal ions. Based on this assumption, we first tested the influence of common metal ions on the luminescence intensity of the Tb^{3+}-XO-DPA system. It was necessary to determine the concentration of DPA because it was the key to achieving the highest sensitivity. Therefore, to optimize the concentration of DPA, the plot in Fig. 1D was differentiated to obtain the relationship between the differential coefficient and the concentration of DPA. As presented in Fig. S6 (Supporting information), the differential coefficient reached a maximum when the DPA concentration was 28 μmol/L. Theoretically, the higher the differential coefficient, the more drastic is the change in the luminescence intensity at that concentration, which implies a higher sensitivity for the detection of metal ions. Hence, we considered that 28 μmol/L DPA would be conducive to achieving the highest sensitivity. As displayed in Fig. 1F, the addition of Hg^{2+}, Pb^{2+}, Al^{3+}, Cu^{2+} and Zn^{2+} resulted in a sharp decrease in the luminescence intensity, while the others had little influence. The luminescence spectra with the continuous addition of the above five metal ions are presented in Figs. 2A–E, respectively. The luminescence intensity decreased gradually as the concentration of metal ions increased. The plots of the luminescence intensity at 545 nm against the concentration of five metal ions are displayed in Figs. 2F–J, respectively. Here, linear calibration curves could be constructed in the lower Hg^{2+} concentration range of 0 μmol/L to 20 μmol/L, Pb^{2+} concentration range of 0 μmol/L to 1 μmol/L (and 0 μmol/L to 8 μmol/L), Al^{3+} concentration range of 0 μmol/L to 14 μmol/L, Cu^{2+} concentration range of 0 μmol/L to 20 μmol/L, and Zn^{2+} concentration range of 0 μmol/L to 8 μmol/L. The impact of these five metal ions on the UV–vis absorption spectra was also investigated. Interestingly, their influences on colorimetric signals were not the same, as shown in the photograph in Fig. 1F. Under optimum conditions, the UV–vis spectra of the Tb^{3+}/XO/DPA system treated with various concentrations of metal ions are shown in Figs. 3A–E, respectively. The addition of Hg^{2+} had very little influence on the UV–vis spectra and the color of the solution, while the addition of the other four metal ions all resulted in significant changes in the UV–vis spectra and color. The calibration curves of A_{430}/A_{570} against the concentration

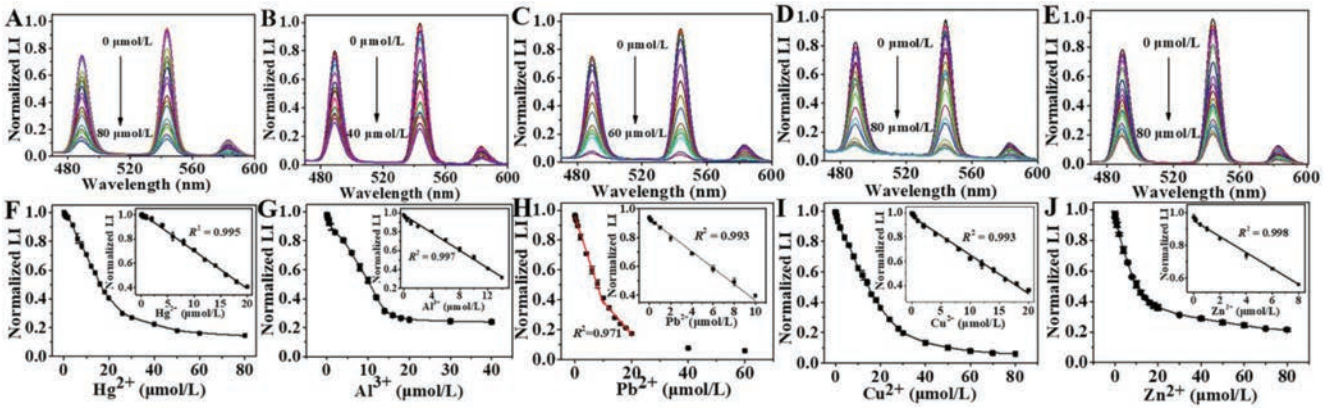

Fig. 2. (A, C, E, G, I) Luminescence spectra of XO-Tb^{3+}-DPA system with consecutive addition of different metal ions (Hg^{2+}, Pb^{2+}, Al^{3+}, Cu^{2+} and Zn^{2+} respectively). (B, D, F, H, J) Plot of luminescence intensity at 545 nm against the concentration of corresponding metal ions and the linear relationship in lower concentration (inset).

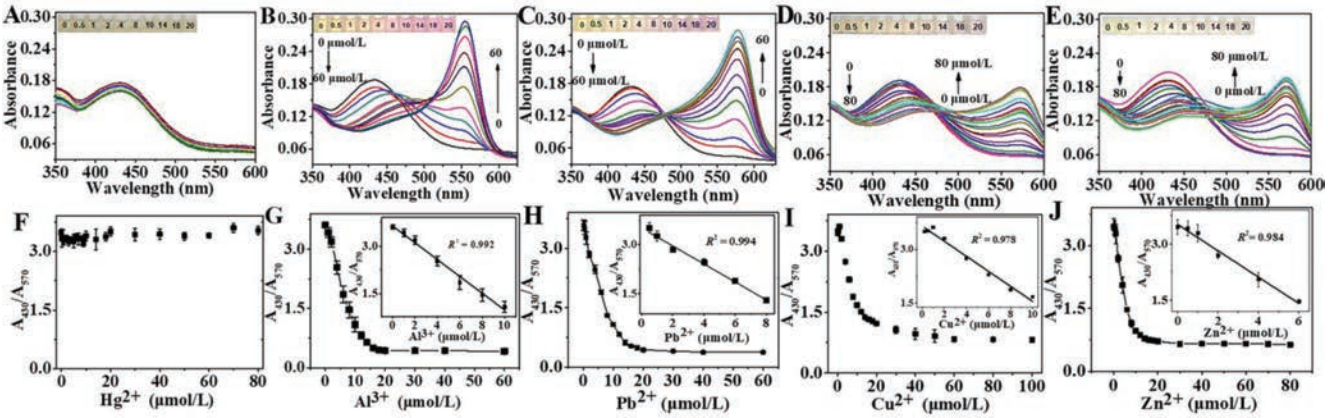

Fig. 3. (A, C, E, G, I) UV–vis spectra of XO-Tb^{3+}-DPA system with consecutive addition of different metal ions (Hg^{2+}, Pb^{2+}, Al^{3+}, Cu^{2+} and Zn^{2+} respectively) and the visual photograph (inset). (B, D, F, H, J) Plot of change in the absorbance ratio (A_{430}/A_{570}) against the concentration of corresponding metal ions and the linear relationship in lower concentration (inset).

of metal ions are also presented in Figs. 3F–J. Note that the color changes caused by the other four kinds of ions were not exactly the same, as also seen in the absorption spectra. The maximum absorption wavelength in the presence of different metal ions was different, especially with Al^{3+}, and the degree of red-shift of the peak at 430 nm also varied. These findings offer the possibility of simultaneously detecting and distinguishing the five metal ions.

Owing to the considerable diversity in terms of the luminometric and colorimetric responses in the presence of these metal ions, linear discriminant analysis (LDA) was used to analyze these patterns. To our knowledge, all reports thus far in the literature related to LDA or principal component analysis (PCA) have been based on sensor arrays requiring several sensing systems [34–36], which is cumbersome and time-consuming. In contrast, LDA here requires only response signals from the same sensing system. For example, metal ions of the same concentration (8 μmol/L) were added to the Tb^{3+}-XO-DPA system. Subsequently, the parameters of luminescent intensity, A_{430}/A_{570}, and the maximum absorption wavelength in the UV–vis spectra were used to conduct LDA. The training matrix (three parameters × five metal ions × six replicates) was converted into four canonical scores, and the first two most significant discrimination factors (89.70% and 8.43%) were applied to produce a 2D canonical plot. As shown in Fig. 4A, the five metal ions generated distinct response patterns and could be separately grouped into different clusters. Because the maximum absorption wavelengths of the system in the presence of Pb^{2+}, Cu^{2+}, and Zn^{2+} were similar, these three ions were relatively close to each

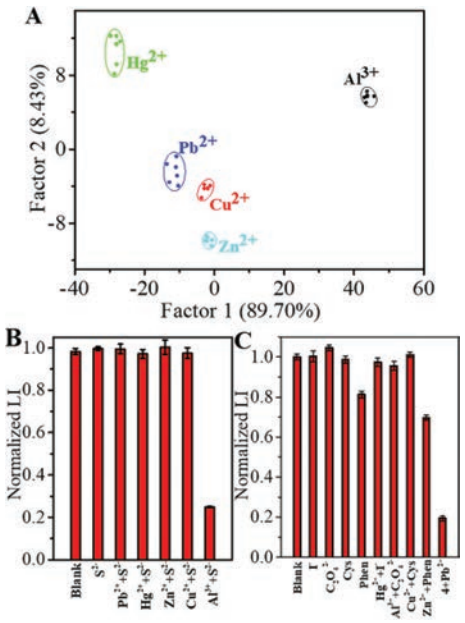

Fig. 4. (A) 2D canonical score plot for the first two factors obtained against 8 μmol/L of metal ions by LDA analysis. The selective detection of Al^{3+} (B) and Pb^{2+} (C) using masking agents ($4 + Pb^{2+}$: $I^- + C_2O_4^{2-} + Cys + Phen + Pb^{2+}$).

other and far away from Hg^{2+} and Al^{3+}. LDA with metal ions at other concentrations (4, 12, and 16 μmol/L) was also carried out, as shown in Fig. S7 (Supporting information). These results confirm that the Tb^{3+}-XO-DPA chemosensor has a strong ability to discriminate between the five metal ions.

In addition, the possibility of specific and sensitive detection of metal ions using masking agents was studied. As shown in Fig. 4B, the addition of S^{2-} could mask the effect of Pb^{2+}, Cu^{2+}, Zn^{2+}, and Hg^{2+} on the luminescence intensity of the system, thus selectively detecting Al^{3+}. The specific detection of Pb^{2+} could be achieved by employing the masking effect of Phen on Zn^{2+}, I^- on Hg^{2+}, Cys on Cu^{2+}, and $C_2O_4^{2-}$ on Al^{3+} (Fig. 4C). Regrettably, no suitable masking agent was found to mask Pb^{2+} alone; therefore, the selective detection of Cu^{2+}, Zn^{2+}, or Hg^{2+} could not be implemented.

With respect to the reasons why these five metal ions present different characteristics, we made the following assumptions. As indicated by the results, the addition of Hg^{2+} failed to cause a color change in the system, making it distinct from the others. Therefore, we speculate that the luminescence quenching mechanism of Hg^{2+} is distinctly different from that of the other four ions. To clarify the mechanism, a more comprehensive control experiment was conducted. The UV–vis absorption spectra of XO alone mixed with different kinds and concentrations of metal ions are shown in Fig. S8 (Supporting information). Except for Hg^{2+}, the addition of the other four metal ions all led to remarkable absorption spectra changes in XO. The maximum absorption wavelength of Al^{3+}-XO occurred at 550 nm, while those of the Pb^{2+}-XO, Cu^{2+}-XO, and Zn^{2+}-XO complexes were all around 570 nm. These clear changes in the absoption spectra demonstrated that the primary coordination form between these four ions with XO was the same as that of Tb^{3+}-XO (Fig. S8F in Supporting information). Although the introduction of Hg^{2+} failed to change the absorption spectrum of XO, considering the strong affinity between $Hg^{2+}$and carboxylate [37], we inferred that Hg^{2+} also formed complexes with XO. However, Hg^{2+} coordinated with the carboxyl oxygen rather than phenolic oxygen, as shown in Fig. S8G (Supporting information). The maximum absorbance at 550 nm caused by Cu^{2+}/Zn^{2+} was lower than that of Al^{3+}/Pb^{2+} at the same concentration; therefore, we speculated that a small part of Cu^{2+}/Zn^{2+} also had the same coordination form as Hg^{2+} with XO. In addition, the effects of metal ions on the absorption peaks of XO were consistent with those of the Tb^{3+}-XO complex, indicating that the added metal ions did not replace Tb^{3+} in the complex, but formed a complex with XO. The case for Hg^{2+} was unique because the absorption spectra remained nearly the same from the beginning to the end. Because the stability constant of Hg^{2+} with DPA is at least three orders of magnitude higher than that of other ions [38], we expect that Hg^{2+} has a super-high affinity for DPA. Therefore, we deduced that a part of the Hg^{2+} occupied the coordination sites of DPA in the Tb^{3+}-DPA complex, which accelerated the nonradiative recombination of excitations *via* the electron transfer process (PET) [38], suppressing the energy transfer from DPA to Tb^{3+} and quenching the luminescence of Tb^{3+}. In contrast, the other four ions (Al^{3+}, Cu^{2+}, Zn^{2+} and Pb^{2+}) coordinated with XO, resulting in a color change. As the maximum absorption peak is located near 570 nm, which is close to the luminescence emission peak at 550 nm, the inner filter effect of luminescence may occur [39], thereby causing luminescence quenching. The degree of luminescence quenching caused by Pb^{2+}/Al^{3+} was greater than that of Cu^{2+}/Zn^{2+} at the same concentration, which also confirms above conjecture.

In summary, the colorimetric and luminometric detection of an anthrax biomarker, DPA, was successfully realized using a novel XO-Tb^{3+} binary complex based on the ligand displacement principle. The dual-readout mode and ratiometric strategy greatly improved the accuracy and sensitivity, with a DPA detection limit as low as 34 nmol/L, making this assay a promising candidate for the real-time detection of pathogenic bacterial spores. Considering the high affinity of the carboxyl group to metal ions, the system enabled the precise discrimination and quantification of five metal ions (Hg^{2+}, Pb^{2+}, Al^{3+}, Cu^{2+} and Zn^{2+}). Such a sensing platform requires a simple mixture of several solutions and allows detection within a very short time, as well as allows the simultaneous detection of multiple substances in the same system. Coupled with its simple operation and extremely fast response time, this assay offers remarkable potential as a sensing platform. We believe that the present study broadens the scope of research on lanthanide complexes and will inspire the development of multifunctional sensing platforms.

Declaration of competing interest

The authors report no declarations of interest.

Acknowledgments

This work was funded by the National Natural Science Foundation of China (No. 21804083) and Youth Innovation Promotion Association of the Chinese Academy of Sciences (No. 2018258).

Supplementary materials

Supplementary material associated with this article can be found, in the online version, at doi:10.1016/j.cclet.2022.02.009.

References

[1] L. Lu, C. Chen, D. Zhao, J. Sun, X. Yang, Anal. Chem. 88 (2016) 1238–1245.
[2] J.C.G. Bünzli, Acc. Chem. Res. 39 (2006) 53–61.
[3] X. Lin, E.L. Ning, X.M. Li, Q.W. Li, Chin. Chem. Lett. 31 (2020) 813–817.
[4] S.V. Eliseeva, J.C.G. Bünzli, Chem. Soc. Rev. 39 (2010) 189–227.
[5] K.J. Hetrick, M.A. Aguilar Ramos, R.T. Raines, Anal. Chem. 91 (2019) 8615–8621.
[6] W.H. Wang, Q. Gao, X.Y. Li, et al., Chin. Chem. Lett. 30 (2019) 75–78.
[7] T. Wang, Q. Mei, Z. Tao, et al., Biosens. Bioelectron. 148 (2020) 111791.
[8] H. Ma, K. Chen, B. Song, et al., Biosens. Bioelectron. 168 (2020) 112560.
[9] H. Gao, P. Zhang, T. Guan, et al., Talanta 231 (2021) 122243.
[10] J. Zhou, H. Li, H. Zhang, et al., Adv. Mater. 27 (2015) 7072–7077.
[11] M.L. Cable, J.P. Kirby, D.J. Levine, et al., J. Am. Chem. Soc. 131 (2009) 9562–9570.
[12] Y. Song, J. Chen, D. Hu, et al., Sensor. Actuat. B: Chem. 221 (2015) 586–592.
[13] L. Guo, M. Liang, X. Wang, et al., Chem. Sci. 11 (2020) 2407–2413.
[14] B. Zhang, H. Wang, L. Lu, et al., Adv. Funct. Mater. 18 (2008) 2348–2355.
[15] C. Huang, R. Ma, Y. Luo, et al., Anal. Chem. 92 (2020) 12934–12942.
[16] M. Cheung, W.W. Lee, D.P. Cowcher, R. Goodacre, S.E. Bell, Chem. Commun. (Camb) 52 (2016) 9925–9928.
[17] N. Bhardwaj, S. Bhardwaj, J. Mehta, K.H. Kim, A. Deep, Biosens. Bioelectron. 86 (2016) 799–804.
[18] K. Luan, R. Meng, C. Shan, et al., Anal. Chem. 90 (2018) 3600–3607.
[19] M.D. Yilmaz, H.A. Oktem, Anal. Chem. 90 (2018) 4221–4225.
[20] G. Wang, Z. Cai, X. Dou, Cell Rep. Phys. Sci. 2 (2021) 100317.
[21] Q.X. Wang, S.F. Xue, Z.H. Chen, et al., Biosens. Bioelectron. 94 (2017) 388–393.
[22] M. Donmez, M.D. Yilmaz, B. Kilbas, J. Hazard. Mater. 324 (2017) 593–598.
[23] N. Gao, Y. Zhang, P. Huang, et al., Anal. Chem. 90 (2018) 7004–7011.
[24] Y. Zhou, X. Huang, X. Hu, et al., Biosens. Bioelectron. 190 (2021) 113386.
[25] S.H. Fan, J. Shen, H. Wu, K.Z. Wang, A.G. Zhang, Chin. Chem. Lett. 26 (2015) 580–584.
[26] K.J. Clear, S. Stroud, B.D. Smith, Analyst 138 (2013) 7079–7082.
[27] M.S. Shivakiran, M. Venkataramana, P.V. Lakshmana Rao, Appl. Microbiol. Biotechnol. 100 (2016) 893–901.
[28] J.J. Pang, R.H. Du, X. Lian, et al., Chin. Chem. Lett. 32 (2021) 2443–2447.
[29] Z. Yang, K.Y. Loh, Y.T. Chu, et al., J. Am. Chem. Soc. 140 (2018) 17656–17665.
[30] L.K. Truman, S. Comby, T. Gunnlaugsson, Angew. Chem. Int. Ed. 51 (2012) 9624–9627.
[31] E. Norkus, I. Stalnionien, D.C. Crans, Heteroat. Chem. 14 (2003) 625–632.
[32] S. Murakami, T. Yoshino, Talanta 28 (1981) 623–625.
[33] C. Liu, Y. Wang, X. Chi, S. Liang, S. Liang, Acta Chim. Si. 47 (1989) 563–568.
[34] L. Qin, X. Wang, Y. Liu, H. Wei, Anal. Chem. 90 (2018) 9983–9989.
[35] H. Yang, F. Lu, Y. Sun, Z. Yuan, C. Lu, Anal. Chem. 90 (2018) 12846–12853.
[36] X. Zhou, T. Wang, M. Zhao, et al., Sensor. Actuat. B: Chem. 343 (2021) 130107.
[37] C.C. Huang, Z. Yang, K.H. Lee, H.T. Chang, Angew. Chem. Int. Ed. 46 (2007) 6824–6828.
[38] H. Tan, B. Liu, Y. Chen, ACS Nano 6 (2012) 10505–10511.
[39] X. Yan, H. Li, X. Han, X. Su, Biosens. Bioelectron. 74 (2015) 277–283.